

Long-range transport of Saharan dust to northern Europe: The 11–16 October 2001 outbreak observed with EARLINET

Albert Ansmann,¹ Jens Bösenberg,² Anatoli Chaikovsky,³ Adolfo Comerón,⁴
Sabine Eckhardt,⁵ Ronald Eixmann,⁶ Volker Freudenthaler,⁷ Paul Ginoux,⁸
Leonce Komguem,⁹ Holger Linné,² Miguel Ángel López Márquez,⁴ Volker Matthias,²
Ina Mattis,¹ Valentin Mitev,¹⁰ Detlef Müller,¹ Svetlana Music,¹¹ Slobodan Nickovic,¹¹
Jacques Pelon,¹² Laurent Sauvage,¹³ Piotr Sobolewsky,¹⁴ Manoj K. Srivastava,¹⁰
Andreas Stohl,⁵ Omar Torres,¹⁵ Geraint Vaughan,⁹ Ulla Wandinger,¹
and Matthias Wiegner⁷

Received 9 May 2003; revised 5 August 2003; accepted 5 September 2003; published 24 December 2003.

[1] The spread of mineral particles over southwestern, western, and central Europe resulting from a strong Saharan dust outbreak in October 2001 was observed at 10 stations of the European Aerosol Research Lidar Network (EARLINET). For the first time, an optically dense desert dust plume over Europe was characterized coherently with high vertical resolution on a continental scale. The main layer was located above the boundary layer (above 1-km height above sea level (asl)) up to 3–5-km height, and traces of dust particles reached heights of 7–8 km. The particle optical depth typically ranged from 0.1 to 0.5 above 1-km height asl at the wavelength of 532 nm, and maximum values close to 0.8 were found over northern Germany. The lidar observations are in qualitative agreement with values of optical depth derived from Total Ozone Mapping Spectrometer (TOMS) data. Ten-day backward trajectories clearly indicated the Sahara as the source region of the particles and revealed that the dust layer observed, e.g., over Belsk, Poland, crossed the EARLINET site Aberystwyth, UK, and southern Scandinavia 24–48 hours before. Lidar-derived particle depolarization ratios, backscatter- and extinction-related Ångström exponents, and extinction-to-backscatter ratios mainly ranged from 15 to 25%, –0.5 to 0.5, and 40–80 sr, respectively, within the lofted dust plumes. A few atmospheric model calculations are presented showing the dust concentration over Europe. The simulations were found to be consistent with the network observations. **INDEX TERMS:** 0305 Atmospheric Composition and Structure: Aerosols and particles (0345, 4801); 0368 Atmospheric Composition and Structure: Troposphere—constituent transport and chemistry; 0933 Exploration Geophysics: Remote sensing; 1630 Global Change: Impact phenomena; **KEYWORDS:** mineral dust, lidar network

Citation: Ansmann, A., et al., Long-range transport of Saharan dust to northern Europe: The 11–16 October 2001 outbreak observed with EARLINET, *J. Geophys. Res.*, 108(D24), 4783, doi:10.1029/2003JD003757, 2003.

1. Introduction

[2] Long-range transport of desert dust mainly takes place in the free troposphere [Carlson and Prospero, 1972;

Prospero et al., 1981; Hamonou et al., 1999; Murayama et al., 2001; Mattis et al., 2002]. As a consequence, ground-based and spaceborne passive remote sensing cannot be used to quantify the radiative effects of these mineral dust particles accurately. Critical assumptions on the com-

¹Leibniz-Institut für Troposphärenforschung, Leipzig, Germany.

²Max-Planck-Institut für Meteorologie, Hamburg, Germany.

³Institute of Physics, National Academy of Sciences of Belarus, Minsk, Belarus.

⁴Universitat Politècnica de Catalunya, Barcelona, Spain.

⁵Technische Universität München, Freising-Weihenstephan, Germany.

⁶Leibniz-Institut für Atmosphärenphysik, Kühlungsborn, Germany.

⁷Meteorologisches Institut, Universität München, Munich, Germany.

⁸Geophysical Fluid Dynamics Laboratory, NOAA, Princeton, New Jersey, USA.

⁹Physics Department, University of Wales, Aberystwyth, United Kingdom.

¹⁰Observatoire Cantonal, Neuchâtel, Switzerland.

¹¹Euro-Mediterranean Center on Insular Coastal Dynamics, University of Malta, Valletta, Malta.

¹²Service d'Aéronomie du CNRS, Université Pierre et Marie Curie, Paris, France.

¹³Institute Pierre Simon Laplace, Laboratoire de la Météorologie Dynamique, Palaiseau, France.

¹⁴Institute of Geophysics, Polish Academy of Sciences, Warsaw, Poland.

¹⁵NASA Goddard Space Flight Center, Greenbelt, Maryland, USA.

position and size distributions of the boundary-layer aerosol and of the lofted particles prohibit a proper separation of the boundary-layer optical depth and of the dust-layer optical depth [Sokolik *et al.*, 2001]. Because of poor knowledge of the surface reflectance characteristics, which vary with daytime and season, thin dust plumes often remain undetected over continents when visible wavelengths are used in the retrieval. Dust also often remains unresolved when the outbreaks are associated with cloud (cirrus) formation.

[3] In view of these shortcomings complementary approaches to column-integrated observations are strongly required. Lidar networks such as the Asian dust network [Murayama *et al.*, 2001] and the European Aerosol Research Lidar Network (EARLINET) [Bösenberg *et al.*, 2001b] seem to be most appropriate for an adequate monitoring of long-range dust transports. Only active remote sensing permits a clear separation of optical effects caused by boundary layer aerosols and lofted dust plumes on a routine and continuous basis and thus allows a quantitative description of complex aerosol layering typically related to these aerosol outbreaks [Müller *et al.*, 2003]. The advantage of lidar was demonstrated during several field campaigns dedicated to investigate pollution outbreaks from continents [Redemann *et al.*, 1998, 2000; Flamant *et al.*, 2000; Ansmann *et al.*, 2002; Wandinger *et al.*, 2002; Pelon *et al.*, 2002; Franke *et al.*, 2003].

[4] According to the latest report by the *Intergovernmental Panel on Climate Change* (IPCC) [2001], dust causes large uncertainties with respect to the assessment of climate forcing by atmospheric aerosols. Sokolik *et al.* [2001] mentioned that the existing uncertainties are caused in part by the limited data on dust climatology (i.e., spatial pattern of dust distribution) and our incomplete understanding of the processes responsible for the production, transport, physical and chemical evolution, and removal of mineral aerosols at various space scales and timescales. Therefore a key issue of EARLINET is the observation of transport of Saharan dust across Europe. In fact, the regular observations by the EARLINET stations showed frequent advection of Saharan dust to southern Europe and occasionally (3–5 times per year) to the northern stations [Papayannis *et al.*, 2002].

[5] A long-range dust transport to the northern parts of Europe observed with EARLINET is presented here. For the first time, an optically dense Saharan dust layer was documented with high vertical and horizontal resolution on a continental scale. The major Saharan dust outbreak occurred in October 2001. The northward spread of the dust particles was observed at 14 out of the 20 EARLINET stations from 11 to 16 October 2001. The measurements taken at 10 stations are presented in this paper.

[6] The paper is organized as follows. After a brief discussion of the EARLINET project and instrumentation in section 2, the dust observations are presented in section 3. Weather charts and satellite imagery are used to explain the general weather conditions and air flow pattern during the dust episode. Backward trajectories were calculated with the 3-dimensional trajectory model FLEXTRA [Stohl *et al.*, 1995] for each EARLINET station up to 10 km height with a vertical resolution of 250 m and a temporal resolution of 3 hours to trace back the observed dust layers to the source region. The lidar data are discussed in terms of profiles of

the particle backscatter coefficient, dust optical depth, depolarization ratio, extinction-to-backscatter ratio (lidar ratio), and Ångström exponent calculated from spectrally resolved backscatter and extinction coefficients. Optical depth maps derived from Total Ozone Mapping Spectrometer (TOMS) data [Torres *et al.*, 1998, 2002] are shown for comparison. A few model results calculated with the Global Ozone Chemistry Aerosol Radiation and Transport (GOCART) model [Ginoux *et al.*, 2001] and the Dust Regional Atmospheric Modelling (DREAM) model [Nickovic *et al.*, 2001] are presented and are found to be consistent with the measurements. The three-dimensional lidar observations provide an almost ideal case for a detailed comparison with regional dust modeling. This is done in a separate paper that is in preparation.

2. EARLINET Instrumentation

[7] EARLINET is a joint project of presently more than 20 European lidar stations. Each lidar group performs observations on a routine base three times a week on preselected days and times since May 2000. EARLINET continued the regular observations of the German lidar network that started in September 1997 [Bösenberg *et al.*, 2001a]. The aim of EARLINET is to establish a quantitative data base of both horizontal and vertical distribution of aerosols on a continental scale [Bösenberg *et al.*, 2001b]. In addition to the regular observations, lidar measurements are performed quasi continuously over longer time periods during so-called special events such as Saharan dust outbreaks, days with a pronounced diurnal cycle of the boundary layer aerosol, and episodes with long and medium-range transport of anthropogenic aerosol, e.g., aerosols originating from forest fires from North America or Arctic haze from polar regions. One of the EARLINET goals was to demonstrate that routine lidar observations are possible over several years in the framework of a large network. The experience made in the framework of the EARLINET project may be used for the installation of future networks in other continents.

[8] The institutions participating in EARLINET in October 2001 are listed in Table 1. EARLINET covers an area from 58.4°N (Linköping, Sweden) to 37.9°N (Athens, Greece) and from 4.1°W (Aberystwyth, Wales) to 27.4°E (Minsk, Belarus). A map showing the distribution of lidar sites over Europe is given in the next section. Some information about the lidar systems involved in this specific study is summarized in Table 2.

[9] Most systems are multiwavelength lidars which allow us to determine the particle backscatter coefficient β at several wavelengths. From these observations the backscatter-related Ångström exponent k_β , defined by $\beta_1/\beta_2 = (\lambda_1/\lambda_2)^{-k_\beta}$ with wavelength λ , can be determined. The Ångström exponent describes the spectral dependence of the backscatter coefficient. The exponent is typically below 0.5 for large dust particles whereas it is >1 for anthropogenic particles.

[10] At several stations the signal components parallel and perpendicular with respect to the plane of polarization of the transmitted, linearly polarized laser light are detected. The ratio of the cross-polarized to the co-polarized signal is defined as the depolarization ratio. This quantity provides a rather clear signature of desert dust [Murayama *et al.*, 1999;

Table 1. EARLINET Lidar Sites, Coordinates, and Institutions (From North to South)

EARLINET Site		Institution
LK	Linköping, Sweden (58.4°N, 15.6°E)	Försvarets Forskningsanstalt
KB	Kühlungsborn, Germany (54.1°N, 11.8°E)	Leibniz-Institut für Atmosphärenphysik
MI	Minsk, Belarus (53.9°N, 27.4°E)	Institute of Physics, National Academy of Sciences of Belarus
HH	Hamburg, Germany (53.6°N, 10.0°E)	Max-Planck-Institut für Meteorologie
AB	Aberystwyth, United Kingdom (52.4°N, 4.1°W)	Physics Department, University of Wales
BE	Belsk, Poland (51.5°N, 20.5°E)	Institute of Geophysics, Polish Academy of Sciences
LE	Leipzig, Germany (51.4°N, 12.4°E)	Leibniz-Institut für Troposphärenforschung
PL	Palaiseau, France (48.6°N, 2.2°E)	Laboratoire de Météorologie Dynamique, IPSL
MU	Munich, Germany (48.2°N, 11.6°E)	Meteorologisches Institut, Universität München
GP	Garmisch Partenkirchen, Germany (47.6°N, 11.1°E)	Forschungszentrum Karlsruhe
NE	Neuchâtel, Switzerland (47.0°N, 7.0°E)	Observatoire Cantonal
JU	Jungfrauoch, Switzerland (46.5°N, 8.0°E)	Ecole Polytechnique Fédérale de Lausanne
LA	L'Aquila, Italy (42.4°N, 13.6°E)	Dipartimento di Fisica, Università degli Studi dell'Aquila,
BA	Barcelona, Spain (41.4°N, 2.2°E)	Universitat Politècnica de Catalunya
NA	Naples, Italy (40.8°N, 14.3°E)	Istituto Nazionale per la Fisica della Materia
PO	Potenza, Italy (40.6°N, 15.7°E)	Istituto di Metodologie Avanzate di Analisi Ambientale, CNR
TH	Thessaloniki, Greece (40.4°N, 22.9°E)	Aristoteleio Panepistimio Thessalonikis
LC	Lecce, Italy (40.3°N, 18.1°E)	Istituto Nazionale per la Fisica della Materia, Unità di Lecce
LI	Lisbon, Portugal (38.7°N, 9.2°W)	Instituto Superior Técnico
AT	Athens, Greece (37.9°N, 23.6°E)	Ethnikon Metsovion Polytechnion Athinon

Gobbi *et al.*, 2000; Chazette *et al.*, 2001]. Dust depolarization ratios at 532 nm typically range from 0.1 to 0.25 whereas anthropogenic particles produce depolarization ratios below 0.05 [Sakai *et al.*, 2002, 2003].

[11] Several Raman lidars were employed to measure the nitrogen Raman signal return at 387 nm (355-nm primary wavelength) and/or 607 nm (532 primary wavelength) in addition to the elastic backscatter signals at the laser wavelengths. From these observations the volume extinction coefficient α and the volume backscatter coefficient of the particles can be determined independently of each other [Ansmann *et al.*, 1992] and which allow us to determine the extinction-to-backscatter ratio (lidar ratio). This quantity is especially sensitive to changes in the shape of the particles. Backscattering is strongly suppressed in the case of non-spherical dust particles (compared to backscattering by spherical droplets) whereas the extinction coefficient is only weakly influenced by the shape effect [Mishchenko *et al.*, 1997; Kalashnikova and Sokolik, 2002; Müller *et al.*, 2003]. Extinction profiling at two wavelengths allow the determination of the extinction-related Ångström exponent k_{α} , defined by $\alpha_1/\alpha_2 = (\lambda_1/\lambda_2)^{-k_{\alpha}}$.

[12] To ensure high-quality, consistent network observations, the EARLINET lidars were intercalibrated in several campaigns [Freudenthaler *et al.*, 2002; Matthias *et al.*, 2002]. Furthermore, the computer codes used to calculate the backscatter coefficients from the elastic backscatter signals [Klett, 1981, 1985; Fernald, 1984; Sasano *et al.*, 1985] as well as the ones used for the determination of backscatter, extinction, and extinction-to-backscatter ratio from the combined elastic-backscatter and Raman signals [Ansmann *et al.*, 1992] were intensively intercompared [Böckmann *et al.*, 2002; Amodeo *et al.*, 2002]. Synthetic lidar signals were used to test the numerical correctness and accuracy of the algorithms as well as the experience of the groups and the limits of the methods.

3. Observations

3.1. Meteorological Setting

[13] A low-pressure trough extending from the Canary Islands to northern Scotland on 8–10 October 2001 initiated

the northward transport of Saharan dust. On 11–12 October a low was present west of Morocco and a high was located over northern Africa and the Mediterranean Sea as shown in Figure 1 (top) for the 700-hPa pressure level (center height of the dust plumes over Europe). This stable weather pattern, which is visible in all weather charts up to the 500 hPa level (5500 m height), caused a massive export of dust from the Sahara to Europe. On 13 October 2001 the high-pressure system moved slowly northward (compare Figure 1 (middle)) and favored the spread of dust over northwestern and central parts of Europe. During the following days the high-pressure ridge extended further to the northeast (compare Figure 1 (bottom)) so that the African air masses reached southern Sweden and eastern parts of central Europe.

[14] Figure 2 shows a snapshot of the dust transport to Europe observed on 13 October 2001. The Sea-viewing Wide Field-of-view Sensor (SeaWiFS) image from 13 October 2001 clearly indicates the northward transport of dust. In west-east direction the dust plume extended from Spain to Corsica and Sardinia. Note also, that the northeasterly winds east of Italy (compare Figure 1 (middle)) transported anthropogenic pollution plumes from southeastern Europe to Africa.

Table 2. EARLINET Instrument Parameters: Laser Wavelengths, Depolarization Channel, and Nitrogen Raman Channel^a

Site	Wavelength, nm	Depolarization	Raman
KB	355, 532, 1064	-	387, 607
MI	532, 694	-	-
HH	355, 532, 1064	-	387
AB	355	-	387
BE	532, 694, 1064	-	-
LE	355, 532, 1064	532	387, 607
PL	532, 1064	532	-
MU	355, 532	-	-
NE	532, 1064	532	-
BA	1064	-	-

^aDepolarization channel: yes, wavelength; no channel, -. Nitrogen Raman channel: yes, wavelengths; no, -. Only stations considered in this study are listed.

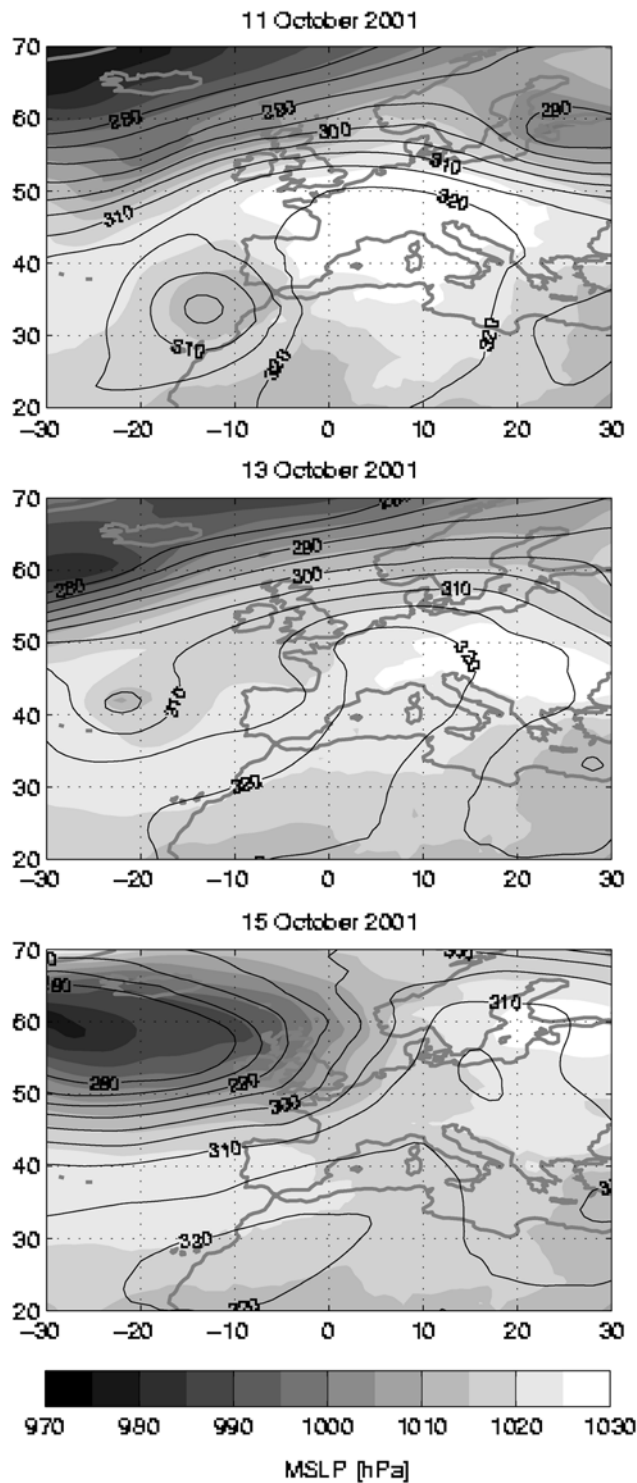


Figure 1. Analyses of the geopotential height at 700 hPa in geopotential decameters (black contour lines) and mean sea level pressure (MSLP; grey shaded contours) on 11, 13, and 15 October 2001 at 1200 UTC based on ECMWF data. The x and y axes show longitude and latitude, respectively.

[15] Figure 2 also includes a sketch of the observed and predicted extent of the dust plume over the western and central parts of Europe on 13 October 2001. Also shown are

the EARLINET lidar stations. We estimated the dust distribution from the SeaWiFS image and backward trajectories.

3.2. Dust Profiles, Optical Depths, and Backward Trajectories

[16] Figure 3 gives an overview of the EARLINET dust observations in terms of the volume backscatter coefficient. The respective volume extinction coefficients in Mm^{-1}

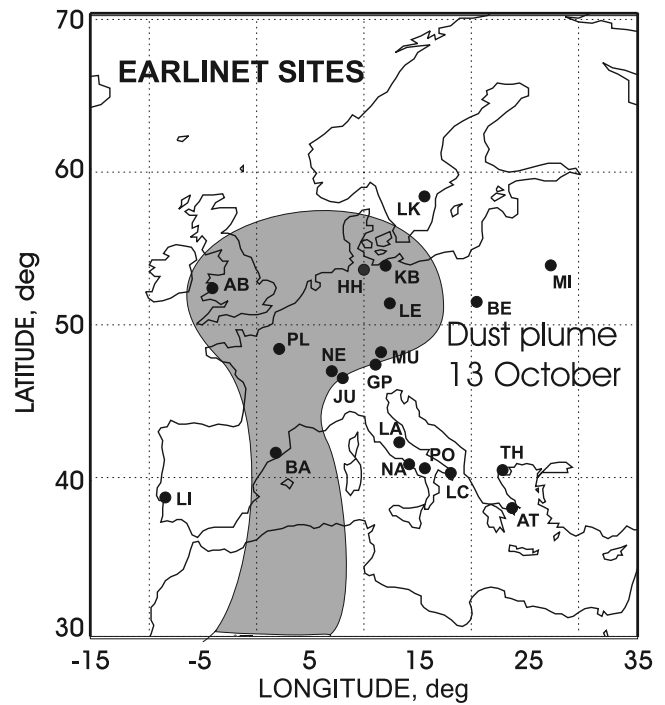
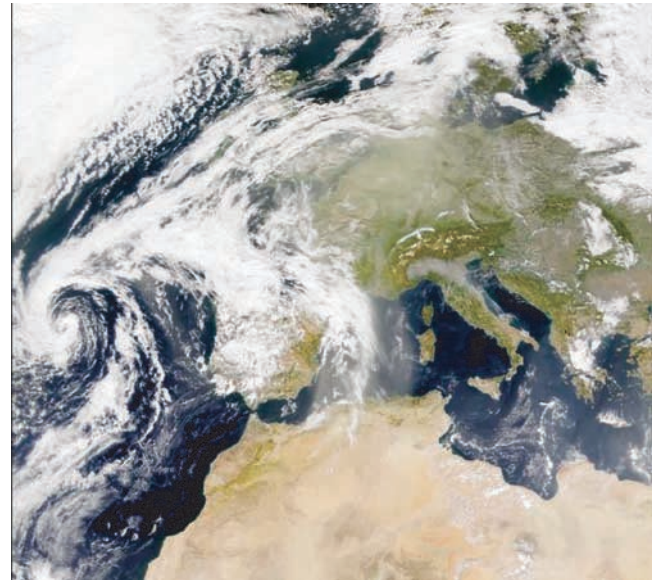


Figure 2. (top) Dust over western and central Europe on 13 October 2001 as seen by SeaWiFS (http://visibleearth.nasa.gov/data/ev102/ev10286_S2001286.L1A_HROM_DUN_CAN.EuropeDust.png) and (bottom) EARLINET sites (compare Table 1). The dust distribution (shaded area) is estimated from the SeaWiFS image.

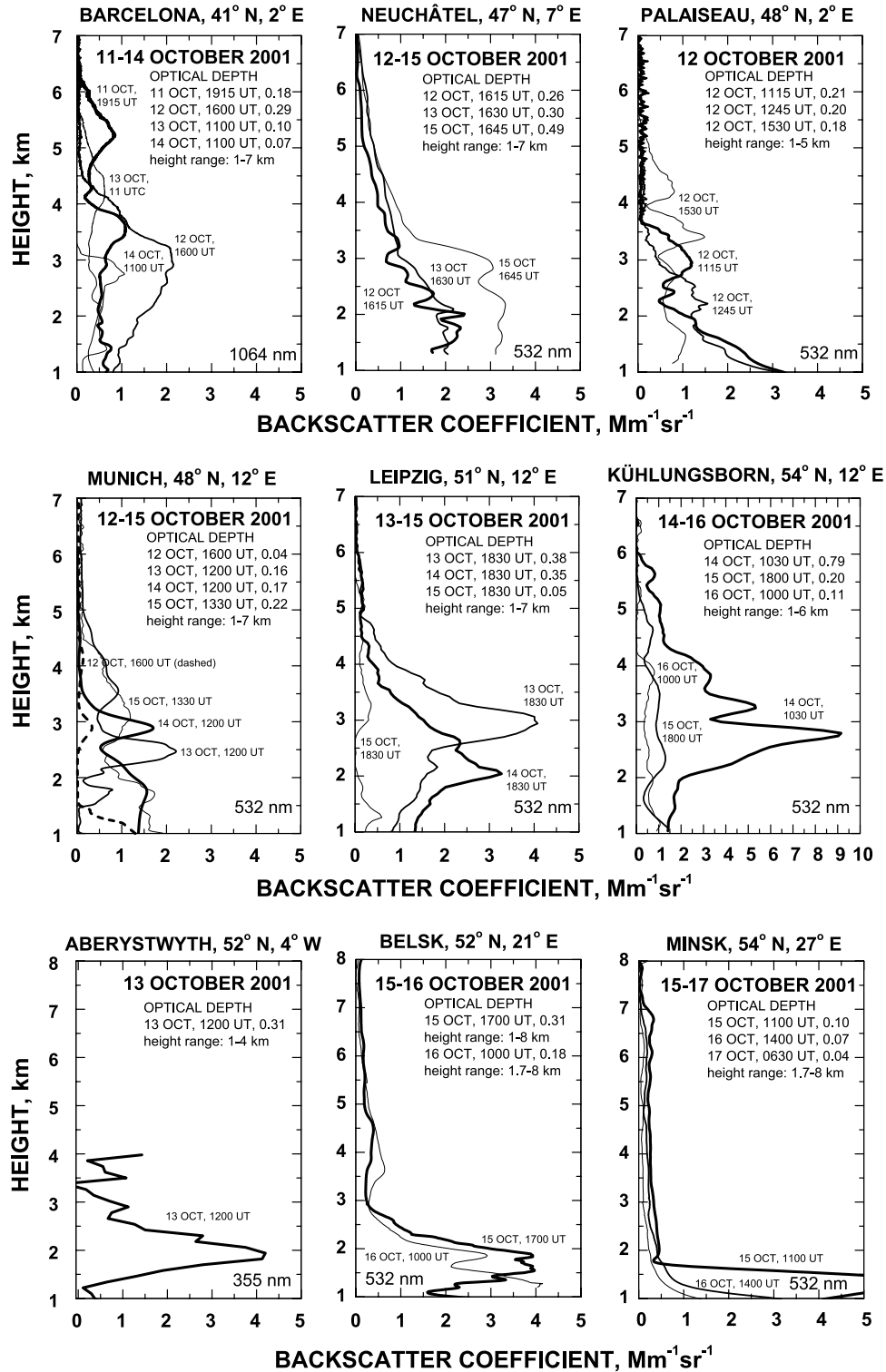


Figure 3. Vertical structure of the Saharan dust layer observed over nine EARLINET sites above 1 km above sea level in terms of the particle backscatter coefficient on 11–17 October 2001. The optical depth values indicated in the plots are calculated from the respective column backscatter values multiplied by the lidar ratio of 60 sr.

(10^{-3} km^{-1} or 10^{-6} m^{-1}) can be estimated from Figure 3 by multiplying the backscatter coefficients by the lidar ratio of 60 sr. This value of 60 sr seems to be most appropriate for Saharan dust after long-range transport to western and

northern Europe [Mattis *et al.*, 2002; Müller *et al.*, 2003]. The integration of the extinction coefficient up to the dust layer top height yields the particle optical depth as indicated in Figure 3. Because the assumed dust lidar ratio may vary

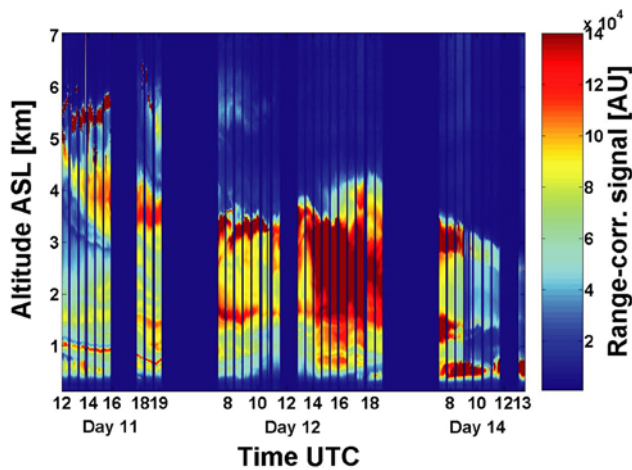


Figure 4. Range-corrected 1064-nm signal (in arbitrary units (AU)) measured at Barcelona, Spain, on 11–14 October 2001. Blue color indicates weak backscattering, and yellow and red colors indicate backscattering mainly by dust particles.

between 40 and 80 sr [Mattis *et al.*, 2002], the uncertainty of the extinction coefficient and optical depth is 25–30%, respectively. The backscatter ratio, defined as the ratio of total to molecular backscattering, can be obtained from the particle backscatter profiles in Figure 3 keeping in mind that the Rayleigh backscatter coefficient is about 1.8–2.6 $\text{Mm}^{-1}\text{sr}^{-1}$ (532 nm), 0.1–0.16 $\text{Mm}^{-1}\text{sr}^{-1}$ (1064 nm), and 9–13 $\text{Mm}^{-1}\text{sr}^{-1}$ (355 nm) for the height range from 0 to 5 km. The backscatter ratio is often used in lidar studies of aerosol, dust and cloud layers.

[17] The base height of the dust layer coincided with the boundary layer top height over most of the stations. The top of the main dust layers reached to heights of 3–5 km. Traces of dust were found up to 7–8 km. The dust optical depth (above 1 km height asl) ranged from about 0.05 to 0.8 at 532 nm. The background particle optical depth of the free troposphere over central Europe is <0.02 at 532 nm as the data measured at Leipzig from 2000 to 2002 indicate. Most impressive in Figure 3 is the strong variability of the vertical distribution of dust within a few hours (Palaiseau) and from day to day (Barcelona, Munich, and Leipzig).

[18] According to the 10-day backward trajectories Saharan dust was transported over distances of 1000–2000 km before arriving at the nearest EARLINET station in Barcelona, Spain. A height-time display of the 1064-nm backscatter signal, observed at Barcelona on 11–14 October 2001 is shown in Figure 4. Data below 500-m height are not trustworthy because of the incomplete overlap between the laser beam and the receiver field of view (RFOV). In contrast to stations further north, plume-like structures resulting from convective processes were still visible. The dust travelled about 2000–3500 km before arriving at Palaiseau near Paris (France), Aberystwyth (Wales), Neuchâtel (Switzerland), and Munich (Germany). The length of the transport path was approximately 5000 km for dust observed over Belsk (Poland) and Minsk (Belarus).

[19] The densest dust clouds (with highest optical depths) moved over eastern Spain (west of Barcelona), western

France, Belgium, The Netherlands, and crossed northern Germany (Hamburg and Kühlungsborn) on 14 October 2001. This result is in agreement with Sun photometer measurements of the Aerosol Robotic Network (AERONET) [Holben *et al.*, 1998]. Cloud-screened particle optical depths of up to 1.2 at 500 nm were recorded at Bordeaux, France, on 12 October 2001 and up to 0.8 were found at Oostende, Belgium, on 13 October 2001.

[20] The backward trajectories for Kühlungsborn on 14 October 2001 are presented in Figure 5. Extremely large backscatter coefficients (compare Figure 3) and extinction coefficients (from Raman lidar observations) of more than 500 Mm^{-1} at 532 nm were found over Kühlungsborn in the late morning of 14 October 2001. The daytime Raman lidar measurement yielded a dust layer optical depth (above 1 km height asl) close to 0.8 and a column-averaged 532-nm lidar ratio of about 60 sr.

[21] Figure 6 shows height-time displays of the 1064-nm range-corrected signal taken at the Baltic Sea lidar station on 14–16 October 2001. The incomplete overlap between laser beam and RFOV (≤ 3 km) is not corrected for in Figure 6. In addition, the 1064-nm channel was overloaded below about 2-km height during the unexpectedly strong dust event on 14 October 2001. As mentioned above, only well-stratified dust layers were observed. Plume-like, convective features as found over Barcelona were absent. Over Kühlungsborn, dust and high-altitude water and ice clouds were often found above each other. The ice clouds formed in North Atlantic air masses. It is not clear whether the water clouds close to the top of the dust layers formed in the African air masses (as a result of lifting processes) or whether these clouds were advected from the North Atlantic. As can be seen in the satellite image of 13 October 2001 in Figure 2, many extended cloud fields were present over the northern parts of Europe.

[22] The lidar observations at Barcelona suggest that this station was east of the main dust transport way. Backward trajectories for Barcelona are shown in Figure 7. The

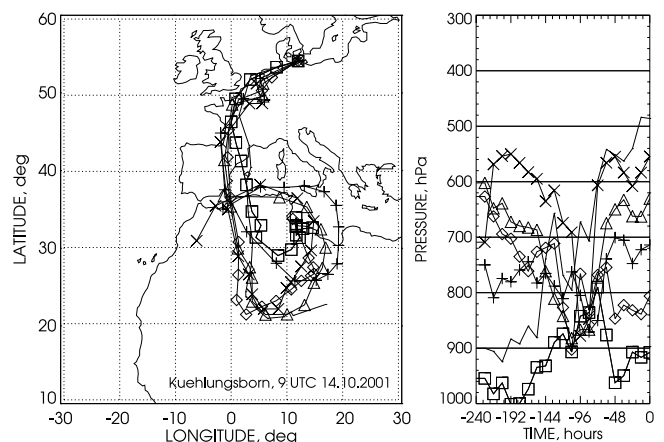


Figure 5. Ten-day backward trajectories for the arrival heights of 1 km (910 hPa), 2 km (810 hPa), 3 km (720 hPa), 4 km (630 hPa), 5 km (550 hPa), and 6 km (480 hPa) above Kühlungsborn, Germany (arrival time: 14 October, 0900 UTC). Only trajectories that crossed northern Africa at heights below 4 km are shown. The time step between individual symbols is 12 hours.

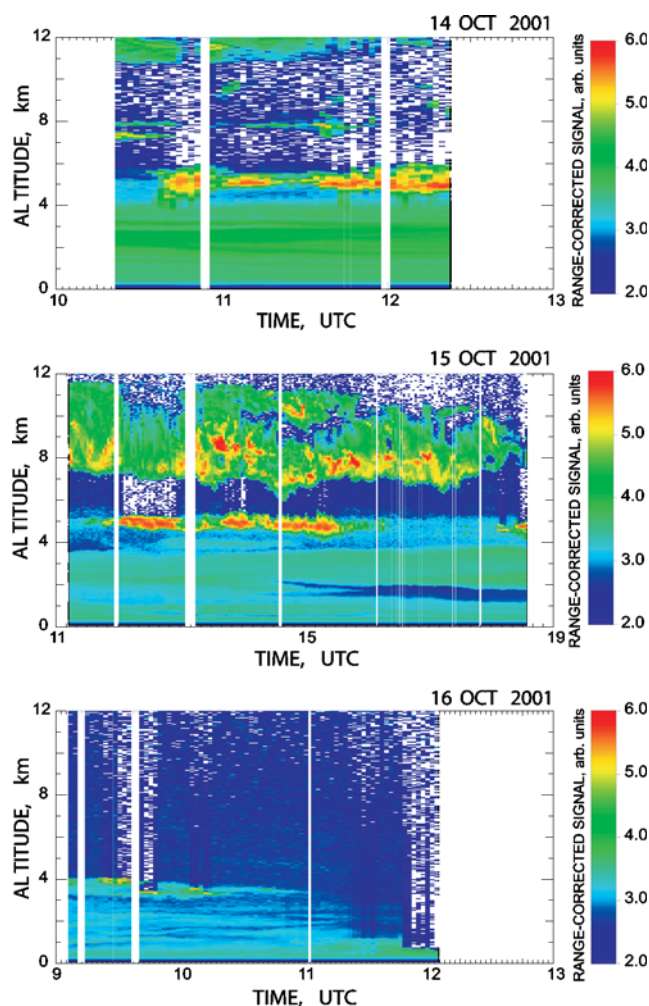


Figure 6. Range-corrected 1064-nm signal measured at Kühlungsborn, Germany, on 14–16 October 2001. Blue color indicates weak backscattering, and green below 6-km height indicates backscattering mainly by dust particles. Water clouds (yellow, red) and cirrus (green to red) were present around 5 km and above 6 km height, respectively, on 14–15 October 2001.

trajectory analysis further revealed that the dust arriving over Barcelona on 11–12 October 2001 travelled to Neuchâtel within 1.5–2 days. The values of the dust optical depth at Neuchâtel are higher than the ones over Barcelona, especially on 15 October 2001. We believe that this is caused in part by anthropogenic particles. Complicated air circulation pattern often prevail over this area, which is surrounded by high mountains. As a consequence, a considerable amount of anthropogenic particles can be lifted to 3–4 km height. The observed relatively low particle depolarization ratios of ≤ 0.1 within the aerosol layers from 1- to 3.5-km height asl on 15 October support the hypothesis of a strong contribution of anthropogenic particles to light extinction above Neuchâtel. The depolarization observations are discussed in more detail below.

[23] Low values of dust optical depths were also found at Palaiseau and Munich (compare Figure 3). The backward trajectories for Munich for the arrival time of 1200 UTC on 13 October 2001 (compare Figure 7) indicate that the air

masses crossed the Paris area (Palaiseau) in the late afternoon and evening of 12 October 2001. The Munich trajectories representing the 2–4-km height range (main dust layers) were above 2000-m over the Saharan desert most of the time. Dust up-take is believed to be weak under such conditions of air flow. This may explain the low dust load and low optical depths over Palaiseau and Munich.

[24] The center plots in Figure 3 (Munich, Leipzig, and Kühlungsborn) give an impression on the south-north cross section of the main part of the dust plume on 14 October. The main part of the dust plume moved in west-east direction on that day. At noon, the dust optical depth (above 1-km-height asl) increased from values below 0.2 at Munich to 0.5 at Leipzig and 0.8 at Kühlungsborn. The dust optical depth at Leipzig decreased slowly with time and reached values of 0.35 in the evening of 14 October as shown in Figure 3. The AERONET Sun photometer at Leipzig measured a particle optical depth of 0.65 at 500 nm at noon of 14 October. The dust backscatter and extinction profiles derived from

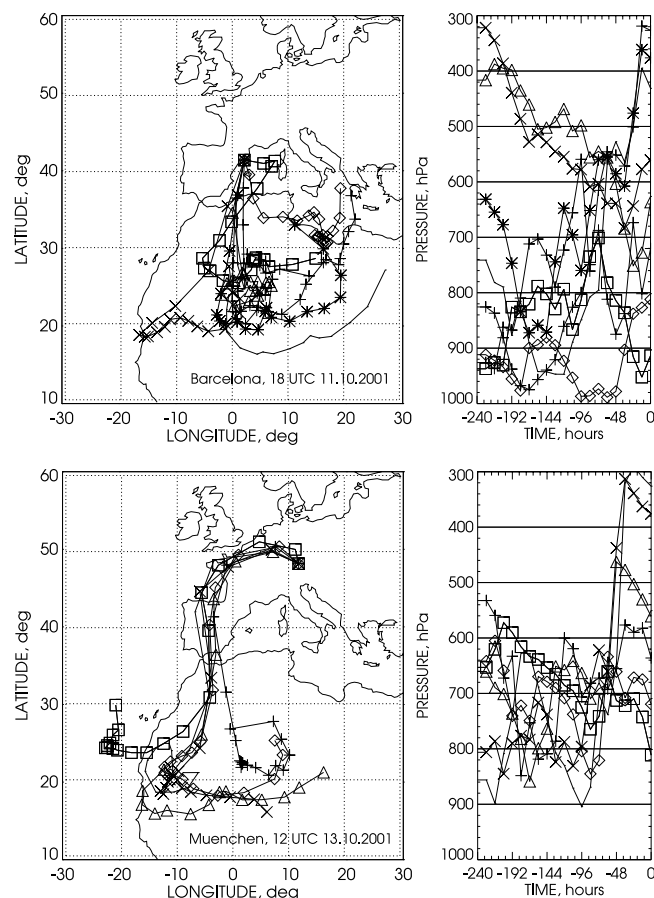


Figure 7. Ten-day backward trajectories arriving (top) over Barcelona, Spain, on 11 October 2001, 1800 UTC and (bottom) over Munich, Germany, on 13 October 2001, 1200 UTC. Arrival heights are 1 km (910 hPa), 2 km (810 hPa), 3 km (720 hPa), 4 km (640 hPa), 5 km (560 hPa), 7 km (430 hPa), 8 km (380 hPa), and 9 km (320 hPa). Only trajectories that crossed northern Africa at heights below 4 km are shown. The time step between individual symbols is 12 hours.

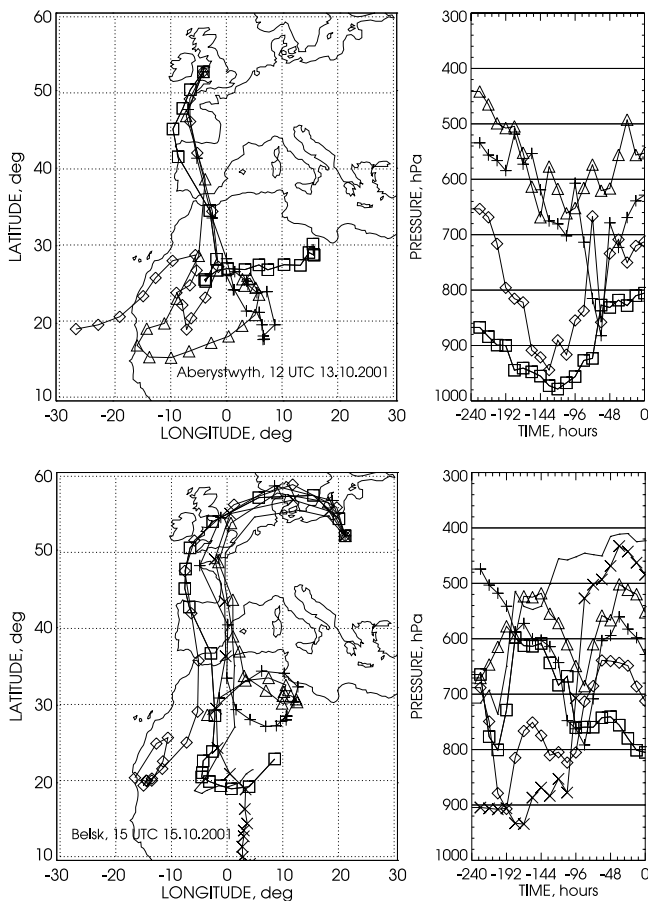


Figure 8. Ten-day backward trajectories arriving (top) over Aberystwyth, UK, on 13 October 2001, 1200 UTC and (bottom) over Belsk, Poland, on 15 October 2001, 1500 UTC. Arrival heights are 2 km (810 hPa), 3 km (720 hPa), 4 km (630 hPa), 5 km (560 hPa), 6 km (480 hPa), and 7 km (420 hPa). Only trajectories that crossed northern Africa at heights below 4 km are shown. The time step between individual symbols is 12 hours.

daytime Raman-lidar observations at Leipzig around noon are discussed in detail by Müller *et al.* [2003].

[25] According to the trajectory analysis for Aberystwyth and Belsk shown in Figure 8, the main dust layers found over these stations below 3-km height travelled over western Spain, and over the North Atlantic west of France to Aberystwyth and then further on to Belsk. A detailed inspection of the trajectories concerning the horizontal and the vertical displacements of the dust plumes revealed that the trajectories that arrived over Belsk at 1600-m and 2500-m height in the afternoon of 15 October were over Aberystwyth at 2000-m and 3000-m height, respectively, 42 hours (2500–3000-height range) and 52 hours (1600–2000-m height range) before. Furthermore, these Belsk and Aberystwyth trajectories showed almost the same transport characteristics over Africa and on the way to Europe, which indicates the same origin of the air mass observed over the two sites. The descent of the dust backscatter maximum by about 400–500 m on the way from Wales to Poland as suggested by the backward trajectory analysis is consistent with the lidar observations in Figure 3. Note that not only

similar dust profile structures but also the same optical depth values were found over Aberystwyth (13 October) and Belsk (15 October).

[26] The backward trajectories for Belsk in Figure 8 also indicate that Saharan dust plumes crossed southern Scandinavia. The dust trajectories that arrived over Minsk at heights above 5 km on 16 October 2001 crossed central Scandinavia at about 65°N. Unfortunately, lidar observations taken at Linköping were strongly disturbed by rainfall. However dust signatures were visible in the range-corrected signals between 2.5- and 4-km height below the main cloud deck. As a result of effective washout, sand was found on cars and window ledges on the evening of 15 October 2001 (R. Persson, Linköping, Sweden, personal communication, 2002).

[27] Figure 9 shows height-time cross sections of the dust plumes for Barcelona, Palaiseau, Leipzig, and Belsk, as estimated from the trajectory data. Each open circle in Figure 9 represents a 10-day backward trajectory that crossed northern Africa at a height below 4 km. We believe that the respective air masses contained dust. Calculations with the dust-cycle model DREAM [Nickovic *et al.*, 2001] support our assumption about the dust up-take over Africa. The modeled meteorological conditions over the Sahara desert forced the dust to move up to about 4–5-km height. According to Figure 9, the dust clouds moved eastward (from Palaiseau to Belsk) with about 35 km per hour or about 800 km per day.

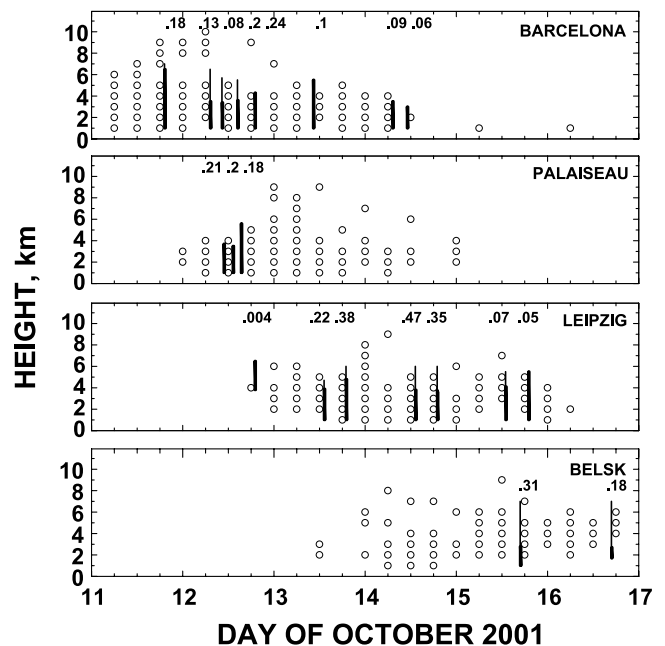


Figure 9. Ten-day backward trajectories (open circles) arriving at Barcelona, Palaiseau, Leipzig, and Belsk, respectively, and indicating dust. All of the marked trajectories crossed northern Africa below 4-km height. Columns (1-km base height) indicate the dust layer as seen by the lidars at the four EARLINET stations. The main dust layer is indicated by a thick vertical line, and thin traces of dust are indicated by a thin line. The optical depths (numbers in the plots) are retrieved from the backscatter coefficients in the same way as described in Figure 3.

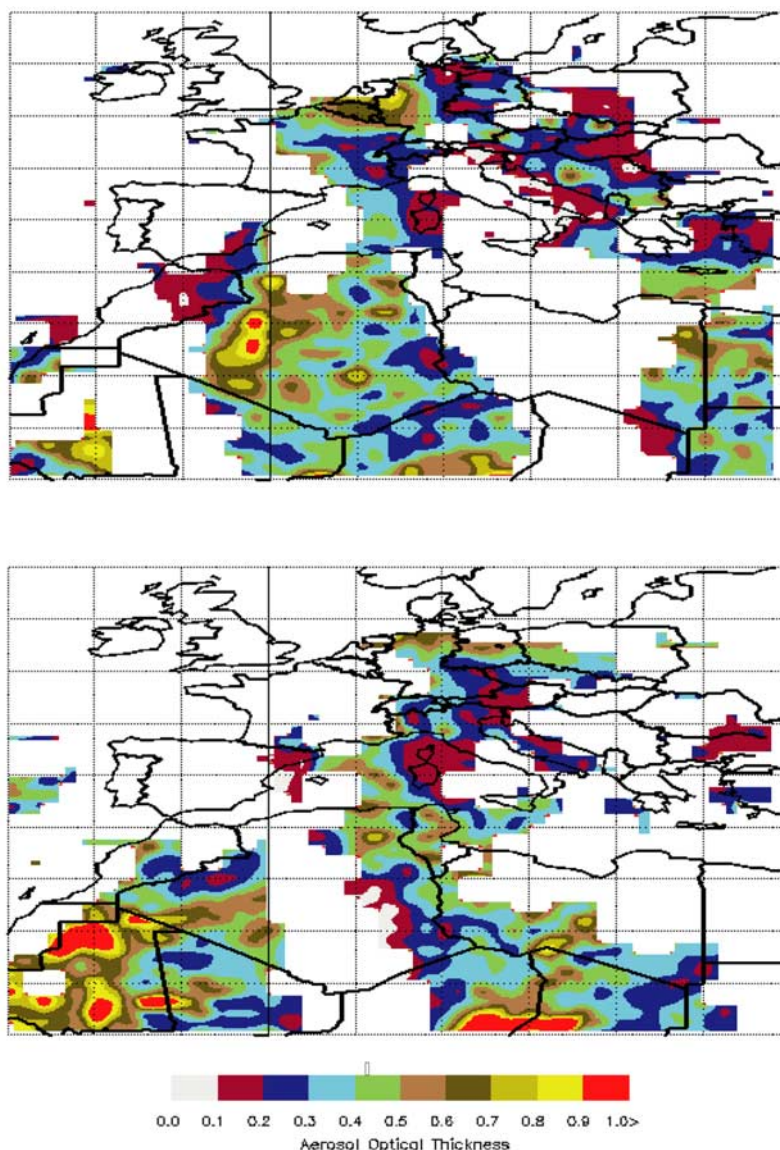


Figure 10. Particle optical depth (380 nm) over northern Africa and Europe retrieved from TOMS observations on (top) 13 October 2001 and (bottom) 14 October 2001. White areas were covered with clouds and could not be analyzed.

[28] Lidar observations, shown in Figure 9 for comparison, are for the most part in good agreement with the trajectory-based dust plumes (compare Leipzig plume). Differences are found for heights above 7 km (compare Barcelona plume). All of these trajectories arriving at heights above 7 km indicate rather strong vertical lifting of the air masses over Africa (compare Barcelona trajectories in Figure 7). Obviously small-scale, convective weather phenomena and frontal passages that may have caused such strong vertical motions were not well enough described (in time and space) in the trajectory model. Meteorological observations (input of the trajectory model) over northern Africa are sparse.

[29] The distribution of total particle optical depth at 380 nm as derived from TOMS data [Torres *et al.*, 1998, 2002] for 13 and 14 October 2001 is shown in Figure 10. In the TOMS data analysis it is assumed that the dust layer

has a Gaussian profile with peak concentration at 3-km height.

[30] As can be seen, the areas with highest optical depth (western central Europe on 13 October, northern Germany on 14 October) are resolved. Despite the fact that clouds considerably disturbed the retrieval and that the optical-depth distribution was rather inhomogeneous, qualitative agreement between the TOMS and EARLINET observations was found in cloud-free regions. TOMS measured total optical depths of 0.2–0.4 over the Munich and Leipzig areas on 13 October 2001 (late morning), whereas the Munich lidar and the Raman lidar at Leipzig measured 0.16 and 0.3 at 532 nm, respectively, for the dust layer above 1-km height at noon. The boundary layer depth was 700–900 m and the particle optical depth of the boundary layer was 0.08–0.12 over Leipzig on 13–14 October 2001 [Müller *et al.*, 2003]. The particle optical depths were about

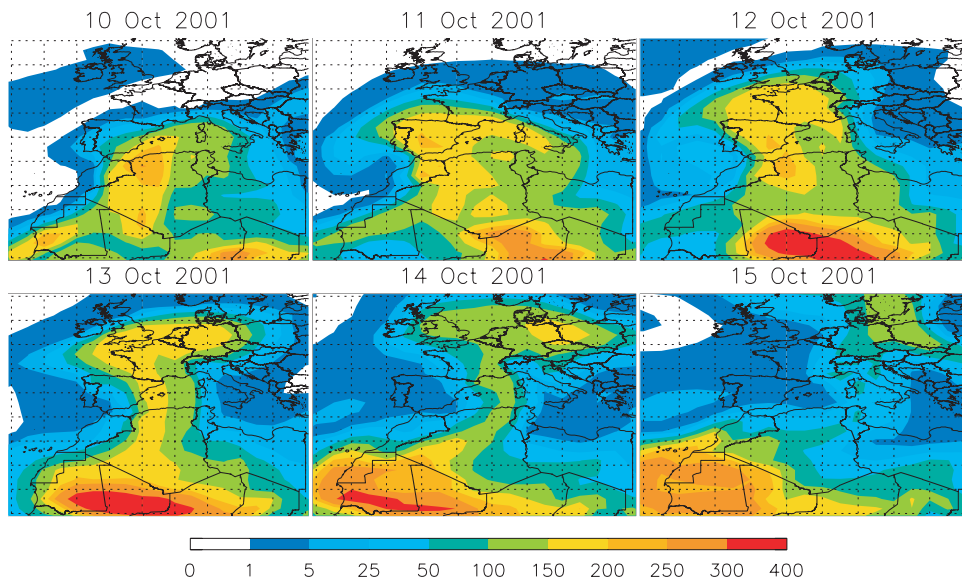


Figure 11. Dust concentration in $\mu\text{g m}^{-3}$ at 2.75-km height above sea level over northern Africa and Europe calculated with the GOCART model.

0.2–0.3, 0.3–0.6, and >0.6 over Munich, Leipzig, and northern Germany, respectively, on 14 October according to TOMS and about 0.2, 0.5, and 0.8 above 1-km height according to the lidars (532-nm wavelength) at Munich, Leipzig, and Kühlungsborn, respectively.

3.3. Model Calculations

[31] The dust outbreak was simulated with the models GOCART and DREAM to provide a more general view of the spread of the dust over Europe. The GOCART results for the 2.75-km height level, i.e., the height of the maximum dust load observed over Kühlungsborn on 14 October (compare Figure 3), are shown in Figure 11. They are consistent with the EARLINET observations, except for Palaiseau and Barcelona. The simulated dust concentrations suggest a dust optical depth much higher than that observed at these stations. As can be seen from Figure 11 the simulations reproduce the southern edge of the densest dust clouds (north of Neuchâtel and Munich) on 13–14 October 2001 and also resolve the high dust load over eastern Germany and western Poland on 14 October. The plume pattern in Figure 11 is in good agreement with the respective distribution of the column mass concentration that was calculated with DREAM for comparison.

[32] Figure 12 presents simulated vertical cross sections of the dust plume in south-north direction for the longitude of 12°E at 1200 and 1800 UTC on 14 October 2001. These calculations were done with DREAM. The simulated plumes can be compared with the lidar observations (compare Figure 3) at Munich (48°N , 12°E , Figure 12, left plot), Leipzig (51°N , 12°E , Figure 12, right plot), and Kühlungsborn (54°N , 12°E , Figure 12, left plot). Qualitative agreement is given concerning the main profile characteristics (pronounced backscatter maximum below 3-km height, top height of the dust layer at about 6 km). The profiles simulated with GOCART showed a less pronounced dust maximum. The maximum dust concentration was about a

factor of 2 lower in the GOCART simulations and the top height was at greater heights (above 8 km).

[33] A more detailed comparison of the simulated results with the EARLINET observations is not possible without an extended discussion of uncertainties in the simulations, observations, and especially in the conversion of lidar-derived optical properties into quantities such as dust concentration and column mass. These discussions will be presented in a follow-up paper based on the detailed comparisons of the lidar profiles with the model outputs.

[34] Because of the central role of these conversion calculations in the comparison of optical measurements and model results the error sources are briefly discussed here. Most lidar stations only measure the particle backscatter coefficient. A height profile of the extinction-to-backscatter ratio is needed to obtain the extinction-coefficient profile. The extinction-to-backscatter ratio depends critically on particle shape and mean particle size. Profiles of the shape and size distribution characteristics are not available and thus have to be estimated. For the conversion of the lidar-derived extinction profile into a dust concentration profile, which can then be compared with modeled profiles, vertically resolved information on the specific extinction coefficient, i.e., of the ratio of extinction coefficient to the dust concentration, is needed for each station. The profile of the specific extinction coefficient strongly depends on the profile of the dust size distribution which is unknown. Dust size distributions after long-range transport are not well documented in the literature.

[35] Published values of the specific extinction coefficient range from 0.4 to $1 \text{ m}^2\text{g}^{-1}$ assuming spherical particles [Teegen and Fung, 1995; Koepke et al., 1997; Hess et al., 1998]. These values correspond to surface-area-weighted mean radii (effective radii) of desert dust size distributions of about 0.8–2 μm . The combined lidar-photometer observations at Leipzig however suggest that the effective radius was between 0.3 and 0.8 μm [Müller et al., 2003] over central Europe so that the extinction-to-mass conversion

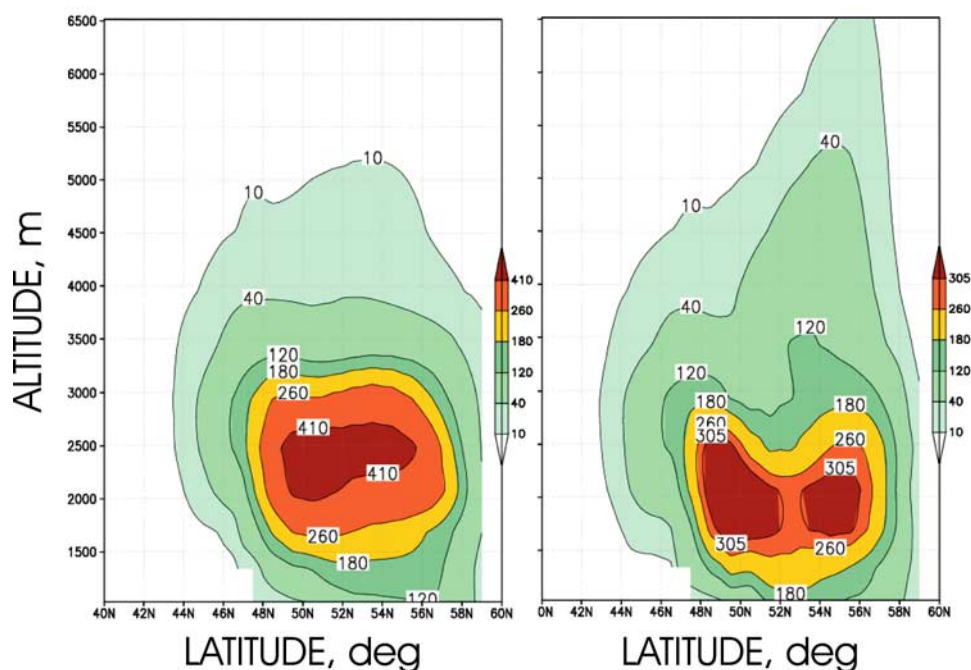


Figure 12. Vertical cross section of the Saharan dust plume in south-north direction for the longitude of 12°E . The DREAM simulation is shown in terms of dust concentration in $\mu\text{g m}^{-3}$ for 14 October 2001, (left) 1200 UTC and (right) 1800 UTC.

ratio should be $1\text{--}3 \text{ m}^2\text{g}^{-1}$ as our Mie scattering calculations show. If we now use these large conversion values we end up with lidar-derived dust concentrations that are roughly a factor of 2–3 lower than the DREAM results in Figure 12. Much better agreement is obtained if we use specific extinction values of $0.2\text{--}0.7 \text{ m}^2\text{g}^{-1}$. However, as mentioned above, because of the unknown input parameters needed in the calculation of the profiles of the extinction-to-backscatter ratio and of the specific extinction coefficients any conclusion concerning possible reasons for the discrepancies is speculative.

3.4. Depolarization Ratio, Ångström Exponent, and Lidar Ratio

[36] Figure 13 shows the EARLINET observations of the particle depolarization ratio, Ångström exponent, and dust lidar ratio. Figure 14 presents the dust evolution over Leipzig in terms of the total (particle + molecule) depolarization ratio at 532 nm above ground. The figure documents that even the tiniest traces of dust are resolved by the depolarization ratio. Well-stratified dust layers were present for several days. Note that the dust penetrated into the boundary layer (top height at 700–800 m) on 14 October 2001.

[37] The Ångström exponents in Figure 13 are calculated from the backscatter coefficients at 532 and 1064 nm, from backscatter coefficients at 355 and 532 nm, and from extinction coefficients derived from Raman lidar signals at 355 and 532 nm. Only profile segments in the dust layers are presented. Because of the highly uncertain calibration of the 1064-nm backscatter profiles, the largest absolute error of about 0.5 is found for the Ångström exponent at the long wavelengths. The retrieval uncertainties are ≤ 0.3 for the other Ångström exponents (355–532-nm region). As

often as possible, cirrus clouds were used for intercalibration, assuming that cirrus backscattering is wavelength-independent.

[38] The quantities shown in Figure 13 allow a better identification of the dust layers and to distinguish them from clouds and anthropogenic aerosol layers. A quantitative interpretation of the profiles in Figure 13 is again not possible because of the complex dependence of the different quantities on unknown particle properties such as chemical composition, particle shape and size distribution and because of the fact that a systematic investigation of the relationship between the shown optical and the underlying physical and chemical properties of the dust particles is not available. Whereas the dust depolarization ratio is believed to be dominated by the influence of the nonspherical shape of the particles, the extinction-related Ångström exponent is mainly a function of particle size and wavelength dependence of the absorption coefficient. The backscatter-related Ångström exponent, on the other hand, is believed to be strongly dependent on particle size and shape. Finally, the lidar ratio varies with changes in the chemical composition (absorption characteristics), the size distributions, and shape characteristics.

[39] Sakai *et al.* [2002] reviewed the literature concerning modeling, laboratory and field studies of the depolarization ratio and Ångström exponents for anthropogenic particles (accumulation mode particles with diameters $\leq 1 \mu\text{m}$) and large maritime and desert dust particles. Anthropogenic and dust particles typically cause depolarization ratios ≤ 0.02 and $0.2\text{--}0.3$, respectively. In agreement with the work of Sakai *et al.* [2002], particle depolarization ratios of $0.2\text{--}0.25$ as found above 1-km height over Leipzig indicate pure dust layers, whereas values from 0 to 0.2 (Palaiseau, Neuchâtel) indicate mixtures of anthropogenic and dust

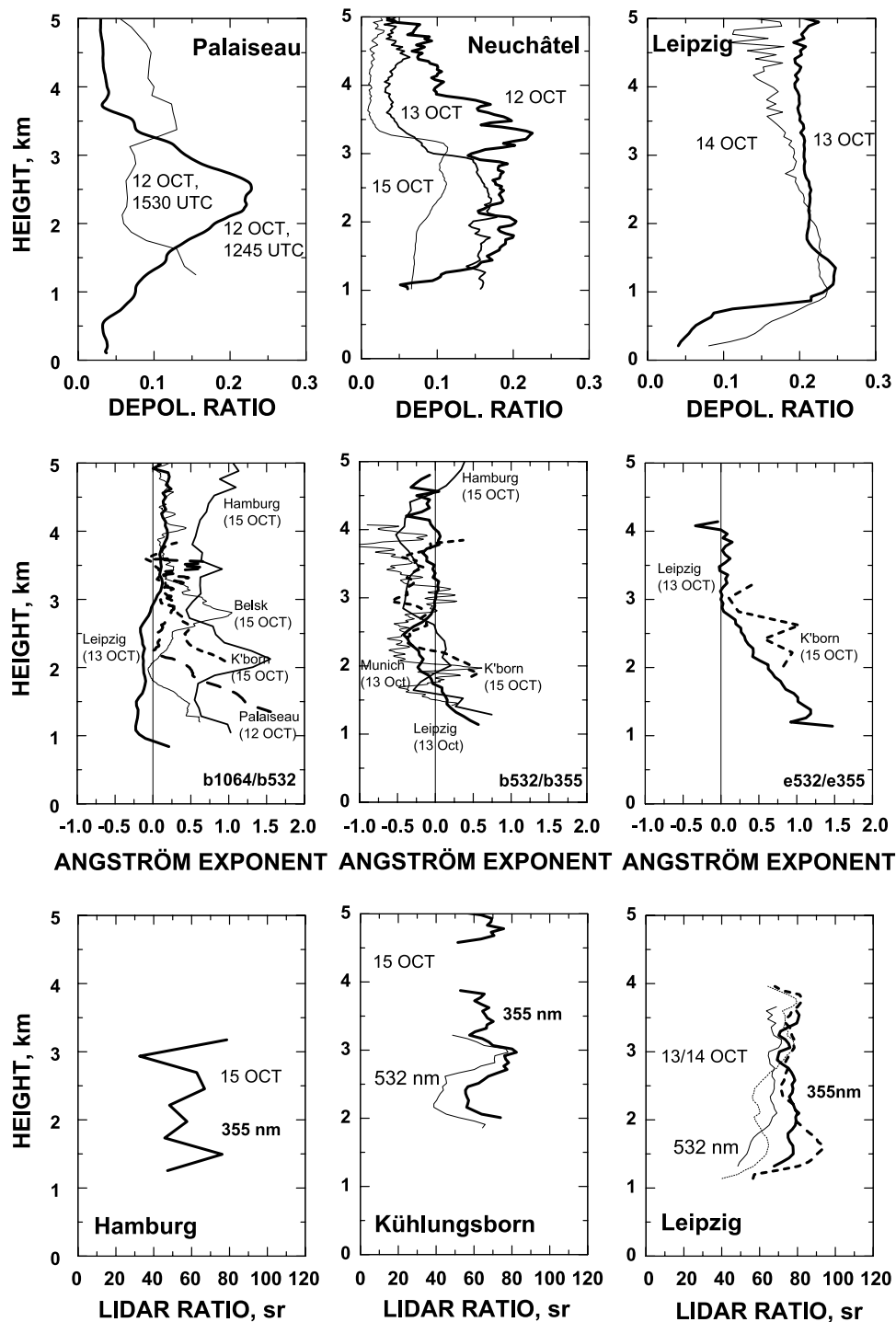


Figure 13. (top) Particle depolarization ratio, (center) Ångström exponent (center left: based on 532 and 1064 backscatter; center: based on 355 and 532 nm backscatter; center right: based on 355 and 532 nm extinction), and (bottom) lidar ratio of Saharan dust. The Ångström plots show data from Leipzig (thick solid lines), Palaiseau (long-dashed lines), Kühlungsborn (K'born, short-dashed lines), Hamburg (medium thick solid lines), Belsk (thin solid lines, left), and Munich (thin solid lines, center).

particles. Thus the increase of the depolarization ratio with height between 500-m and about 2.2-km height (center of the dust layer) over Palaiseau at noon on 12 October suggests a decreasing contribution of scattering and absorption by anthropogenic particles to total extinction. The decrease of the depolarization ratio in the upper part of

the dust plume may again indicate anthropogenic particles. It is also possible that the dust particles became rather small (of comparable size as the anthropogenic particles) or more spherical. Very small particles do not depolarize the incident laser light significantly. The depolarization ratio is zero for spherical particles. Water up-take is, however, less likely

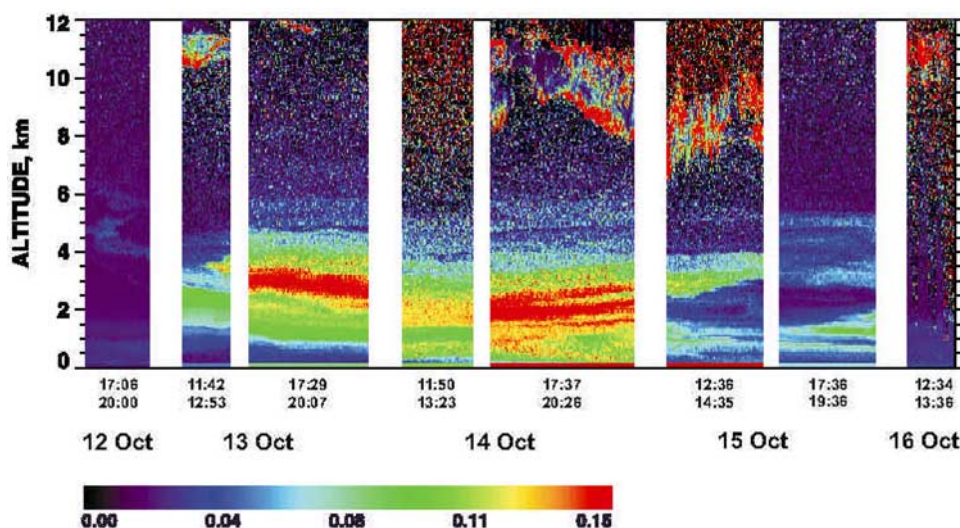


Figure 14. Total (particle + molecule) depolarization ratio observed at Leipzig, Germany, on 12–16 October 2001. Times are in UTC. Below about 6-km height, dust is responsible for high depolarization (green to red). Ice clouds produce high depolarization as well as low depolarization (by specular reflection) at heights above 7-km height.

because of the low relative humidity within the dust layer. The contribution of dust to total light scattering and extinction over Neuchâtel decreased from 12–13 October to 15 October.

[40] The monotonic decrease of the extinction-related Ångström exponent between 1.4- and 2.8-km height over Leipzig in Figure 13 suggest that the mean size of the dust particles monotonically increased with height. The size effect caused a decrease of the Ångström exponent by about 1 within the height range from 1.4 to 2.8 km provided that shape effects had only a minor influence on the Ångström exponent and that the chemical composition and thus the spectral slope of the absorption coefficient did not change with height. As mentioned above it is believed that the 355/532-nm Ångström exponent is determined in part by notable absorption of radiation at 355 nm and negligible absorption at 532 nm.

[41] The backscatter-related Ångström exponent for the short wavelength region shows approximately the same behavior as the extinction-related Ångström exponent in the lower part of the dust layer over Leipzig and supports our hypothesis that the mean particle size increased with height. However, the influence of particle shape on the backscatter-related Ångström exponent cannot be ignored and may have led to the differences between the backscatter and extinction-related Ångström exponents above 2.5-km height.

[42] As can be further seen in Figure 14, most Ångström values for the short wavelength range, measured over the four German EARLINET stations were between 0 and -0.5 . The Ångström exponents for the longer wavelengths (532, 1064 nm) show a quite different behavior. We cannot exclude that the higher uncertainties in the determination of this quantity for the longer wavelengths caused the effect. Wavelength-dependent shape effects in the long wavelength region may also have contributed to the differences. However, we believe that the main reason for the different behavior of the Ångström exponents is the size

distribution of the dust particles. As discussed by Müller *et al.* [2003], the spectral slope of the backscatter and extinctions coefficients in combination with sky radiance and optical depth observations with the AERONET Sun photometer is consistent with dust particles with an effective radius of about 0.3–0.8 μm . Sakai *et al.* [2002] found similar values of the Ångström exponents for the 532–1064-nm region over Japan after long-range transport of dust from the Gobi desert.

[43] Figure 13 also presents a few measurements of the dust extinction-to-backscatter ratio at 355 and 532 nm. Because of signal noise, uncertainties are of the order of 30% in the case of the Hamburg and Kühlungsborn data, and 15% for the Leipzig values. As already discussed elsewhere [Mattis *et al.*, 2002; Müller *et al.*, 2003], it is believed that the lidar ratio is enhanced by a factor of 1.5–3 with respect to the lidar ratio produced by surface-equivalent spheres. Lidar ratios found over Germany at Hamburg, Leipzig, and Kühlungsborn ranged from 50 to 90 sr at 355 nm and 40 to 80 sr at 532 nm. Similar values for the 532-nm lidar ratio is found for Asian dust [Sakai *et al.*, 2002; Liu *et al.*, 2002]. An extended discussion concerning the combined observations of the depolarization ratio, the Ångström exponents, and lidar ratios at Leipzig and additional Sun photometer observations of the particle optical depth spectrum from 340–1020 nm at the AERONET Leipzig site is given by Müller *et al.* [2003].

4. Summary

[44] The spread of dust to northern parts of Europe after a major Saharan dust outbreak has been documented in detail with a lidar network. For the first time the vertical and horizontal distribution of an optically dense dust layer was characterized coherently on a continental scale. Dust was present mainly between 1- and 7-km height, the dust optical depth ranged from 0.1 to 0.8 at 532 nm. Qualitative

agreement was found between TOMS and lidar-derived optical depth values, and between the EARLINET observations and model calculations. Dust depolarization ratios, Ångström exponents, and extinction-to-backscatter ratios within the dust layers mainly ranged from 15 to 25%, -0.5 to 0.5 , and 40 to 80 sr, respectively.

[45] Such three-dimensional observations as presented here are most useful for comparisons with results from dust cycle models because only lidars allow a clear separation of boundary layer aerosols and lofted dust plumes. This is a basic requirement for a trustworthy validation of atmospheric models. Passive remote sensing is of limited use here. In future, spaceborne lidars and ground-based lidar networks in combination with spaceborne and ground-based passive remote sensing will provide us with the required three-dimensional global view of the human impact on the composition and state of the atmosphere, and the role of long-range transport regarding the distribution of aerosols and other pollution.

[46] **Acknowledgments.** This work is supported by the European Commission under grant EVR1-CT1999-40003.

References

- Amodeo, A., et al., Raman lidar algorithm intercomparison in the frame of EARLINET, in *Laser Remote Sensing in Atmospheric and Earth Sciences, Proceedings of the 21st International Laser Radar Conference, Quebec City, Canada*, edited by L. R. Bissonnette, G. Roy, and G. Vallée, pp. 349–352, Def. R&D Can.-Valcartier, Val-Bélair, Que., Canada, 2002.
- Ansmann, A., U. Wandinger, M. Riebesell, C. Weitkamp, and W. Michaelis, Independent measurement of extinction and backscatter profiles in cirrus clouds by using a combined Raman elastic-backscatter lidar, *Appl. Opt.*, **31**, 7113–7131, 1992.
- Ansmann, A., F. Wagner, D. Müller, D. Althausen, A. Herber, W. von Hoyningen-Huene, and U. Wandinger, European pollution outbreaks during ACE 2: Optical particle properties inferred from multiwavelength lidar and star-Sun photometry, *J. Geophys. Res.*, **107**(D15), 4259, doi:10.1029/2001JD001109, 2002.
- Böckmann, C., et al., EARLINET: Backscatter lidar algorithm intercomparison, in *Laser Remote Sensing in Atmospheric and Earth Sciences, Proceedings of the 21st International Laser Radar Conference, Quebec City, Canada*, edited by L. R. Bissonnette, G. Roy, and G. Vallée, pp. 353–356, Def. R&D Can.-Valcartier, Val-Bélair, Que., Canada, 2002.
- Bösenberg, J., et al., The German Aerosol Lidar Network: Methodology, data, analysis, *MPI Rep. 317*, Max-Planck-Inst. für Meteorol., Hamburg, Germany, 2001a.
- Bösenberg, J., et al., EARLINET: A European Aerosol Research Lidar Network, in *Laser Remote Sensing of the Atmosphere, Selected Papers of the 20th International Laser Radar Conference, Vichy, France*, edited by A. Dabas, C. Loth, and J. Pelon, pp. 155–158, École Polytech., Paris, 2001b.
- Carlson, T. N., and J. M. Prospero, The large-scale movement of Saharan air outbreaks over the northern equatorial Atlantic, *J. Appl. Meteorol.*, **11**, 283–297, 1972.
- Chazette, P., J. Pelon, C. Moulin, F. Dulac, I. Carrasco, W. Guelle, P. Bousquet, and P. Flamant, Lidar and satellite retrieval of dust aerosols over the Azores during SOFIA/ASTEX, *Atmos. Environ.*, **35**, 4297–4304, 2001.
- Fernald, F. G., Analysis of atmospheric lidar observations: Some comments, *Appl. Opt.*, **23**, 652–653, 1984.
- Flamant, C., et al., Airborne lidar measurements of aerosol spatial distribution and optical properties over the Atlantic Ocean during a European pollution outbreak of ACE-2, *Tellus, Ser. B*, **52**, 662–677, 2000.
- Franke, K., A. Ansmann, D. Müller, D. Althausen, C. Venkataraman, M. S. Reddy, F. Wagner, and R. Scheele, Optical properties of the Indo-Asian haze layer over the tropical Indian Ocean, *J. Geophys. Res.*, **108**(D2), 4059, doi:10.1029/2002JD002473, 2003.
- Freudenthaler, V., et al., Intercomparison of 21 aerosol lidar systems in the frame of EARLINET, in *Laser Remote Sensing in Atmospheric and Earth Sciences, Proceedings of the 21st International Laser Radar Conference, Quebec City, Canada*, edited by L. R. Bissonnette, G. Roy, and G. Vallée, pp. 297–300, Def. R&D Can.-Valcartier, Val-Bélair, Que., Canada, 2002.
- Ginoux, P., M. Chin, I. Tegen, J. M. Prospero, B. Holben, O. Dubovik, and S.-J. Lin, Sources and distributions of dust aerosols simulated with the GOCART model, *J. Geophys. Res.*, **106**, 20,255–20,273, 2001.
- Gobbi, G. P., F. Barnaba, R. Giorgi, and A. Santacasa, Altitude-resolved properties of a Saharan dust event over the Mediterranean, *Atmos. Environ.*, **34**, 5119–5127, 2000.
- Hamonou, E., P. Chazette, D. Balis, F. Dulac, X. Schneider, E. Galani, G. Ancellet, and A. Papayannis, Characterization of the vertical structure of Saharan dust export to the Mediterranean basin, *J. Geophys. Res.*, **104**, 22,275–22,270, 1999.
- Hess, M., P. Koepke, and I. Schult, Optical properties of aerosols and clouds: The software package OPAC, *Bull. Am. Meteorol. Soc.*, **79**, 831–844, 1998.
- Holben, B. N., et al., AERONET: A federated instrument network and data archive for aerosol characterization, *Remote Sens. Environ.*, **66**, 1–16, 1998.
- Intergovernmental Panel on Climate Change (IPCC), *Climate Change 2001: The Scientific Basis*, edited by J. T. Houghton et al., Cambridge Univ. Press, New York, 2001.
- Kalashnikova, O. V., and I. N. Sokolik, Importance of shapes and composition of wind-blown dust particles for remote sensing at solar wavelengths, *Geophys. Res. Lett.*, **29**(10), 1398, doi:10.1028/2002GLG14947, 2002.
- Klett, J. D., Stable analytical solution for processing lidar returns, *Appl. Opt.*, **20**, 211–220, 1981.
- Klett, J. D., Lidar inversion with variable backscatter/extinction ratios, *Appl. Opt.*, **24**, 1638–1643, 1985.
- Koepke, P., M. Hess, I. Schult, and E. P. Shettle, Global aerosol data set, *MPI Rep. 243*, 44 pp., Max-Planck-Inst. für Meteorol., Hamburg, Germany, 1997.
- Liu, Z., N. Sugimoto, and T. Murayama, Extinction-to-backscatter ratio of Asian dust observed with high-spectral-resolution lidar and Raman lidar, *Appl. Opt.*, **41**, 2760–2767, 2002.
- Matthias, V., et al., Lidar intercomparison on algorithm and system level in the frame of EARLINET, *MPI Rep. 337*, Max-Planck-Inst. für Meteorol., Hamburg, Germany, 2002.
- Mattis, I., A. Ansmann, D. Müller, U. Wandinger, and D. Althausen, Dual-wavelength Raman lidar observations of the extinction-to-backscatter ratio of Saharan dust, *Geophys. Res. Lett.*, **29**(9), 1306, doi:10.1029/2002GL014721, 2002.
- Mishchenko, M. I., L. D. Travis, R. A. Kahn, and R. A. West, Modeling phase functions for dustlike tropospheric aerosols using a shape mixture of randomly oriented polydisperse spheroids, *J. Geophys. Res.*, **102**, 16,831–16,847, 1997.
- Müller, D., I. Mattis, U. Wandinger, D. Althausen, A. Ansmann, O. Dubovik, S. Eckhardt, and A. Stohl, Saharan dust over a central European EARLINET-AERONET site: Combined observations with Raman lidar and Sun photometer, *J. Geophys. Res.*, **108**(D12), 4345, doi:10.1029/2002JD002918, 2003.
- Murayama, T., H. Okamoto, N. Kaneyasu, H. Kamataki, and K. Miura, Application of lidar depolarization measurement in the atmospheric boundary layer: Effects of dust and sea-salt particles, *J. Geophys. Res.*, **104**, 31,781–31,792, 1999.
- Murayama, T., et al., Ground-based network observation of Asian dust events of April 1998 in east Asia, *J. Geophys. Res.*, **106**, 18,345–18,359, 2001.
- Nickovic, S., G. Kallos, A. Papadopoulos, and O. Kakaliagou, A model for prediction of desert dust cycle in the atmosphere, *J. Geophys. Res.*, **106**, 18,113–18,129, 2001.
- Papayannis, A., et al., Two years of continuous observations of Saharan dust events over the European continent using a coordinated LIDAR network in the frame of the EARLINET project, in *Laser Remote Sensing in Atmospheric and Earth Sciences, Proceedings of the 21st International Laser Radar Conference, Quebec City, Canada*, edited by L. R. Bissonnette, G. Roy, and G. Vallée, pp. 349–352, Def. R&D Can.-Valcartier, Val-Bélair, Que., Canada, 2002.
- Pelon, J., C. Flamant, P. Chazette, J.-F. Léon, D. Tanre, M. Sicard, and S. K. Satheesh, Characterization of aerosol spatial distribution and optical properties over the Indian Ocean from airborne lidar and radiometry during INDOEX'99, *J. Geophys. Res.*, **107**(D19), 8029, doi:10.1029/2001JD000402, 2002.
- Prospero, J. M., R. A. Glaccum, and R. T. Nees, Atmospheric transport of soil dust from Africa to South America, *Nature*, **289**, 570–572, 1981.
- Redemann, J., R. P. Turco, R. F. Pueschel, M. A. Fenn, E. V. Browell, and W. B. Grant, A multi-instrument approach for characterizing the vertical structure of aerosol properties: Case studies in the Pacific Basin troposphere, *J. Geophys. Res.*, **103**, 23,287–23,298, 1998.
- Redemann, J., et al., Retrieving the vertical structure of the effective complex index of refraction from a combination of aerosol in situ and remote sensing measurements during TARFOX, *J. Geophys. Res.*, **105**, 9949–9970, 2000.

- Sakai, T., et al., Case study of Raman lidar measurements of Asian dust events in 2000 and 2001 at Nagoya and Tsukuba, Japan, *Atmos. Environ.*, *36*, 5479–5489, 2002.
- Sakai, T., T. Shibata, K. Hara, M. Kido, K. Osada, M. Hayashi, K. Matsunaga, and Y. Iwasaka, Raman lidar and aircraft measurements of tropospheric aerosol particles during the Asian dust event over central Japan: Case study on 23 April 1996, *J. Geophys. Res.*, *108*(D12), 4349, doi:10.1029/2002JD003150, 2003.
- Sasano, Y., E. V. Browell, and S. Ismail, Error caused by using a constant extinction/backscattering ratio in the lidar solution, *Appl. Opt.*, *24*, 3929–3932, 1985.
- Sokolik, I. N., D. M. Winker, G. Bergametti, D. A. Gillette, G. Carmichael, Y. J. Kaufman, L. Gomes, L. Schuetz, and J. E. Penner, Introduction to special section: Outstanding problems in quantifying the radiative impacts of mineral dust, *J. Geophys. Res.*, *106*, 18,015–18,027, 2001.
- Stohl, A., G. Wotawa, P. Seibert, and H. Kromp-Kolb, Interpolation errors in wind fields as a function of spatial and temporal resolution and their impact on different types of kinematic trajectories, *J. Appl. Meteorol.*, *34*, 2149–2165, 1995.
- Tegen, I., and I. Fung, Contribution to the atmospheric mineral aerosol load from land surface modification, *J. Geophys. Res.*, *100*, 18,707–18,726, 1995.
- Torres, O., P. K. Bhartia, J. R. Herman, Z. Ahmad, and J. Gleason, Derivation of aerosol properties from satellite measurements of backscattered ultraviolet radiation: Theoretical basis, *J. Geophys. Res.*, *103*, 17,099–17,110, 1998.
- Torres, O., P. K. Bhartia, J. R. Herman, A. Sinyuk, P. Ginoux, and B. Holben, A long-range record of aerosol optical depth from TOMS observations and comparison to AERONET measurements, *J. Atmos. Sci.*, *59*, 398–413, 2002.
- Wandinger, U., et al., Optical and microphysical characterization of biomass-burning and industrial-pollution aerosols from multiwavelength lidar and aircraft measurements, *J. Geophys. Res.*, *107*(D21), 8125, doi:10.1029/2000JD000202, 2002.
- J. Bösenberg, H. Linné, and V. Matthias, Max Planck Institute for Meteorology, Bundesstraße 55, 20146 Hamburg, Germany. (boesenberg@dkrz.de; linne@dkrz.de; matthias@dkrz.de)
- A. Chaikovsky, Institute of Physics, National Academy of Sciences of Belarus, 68 F. Scarina Avenue, 220072 Minsk, Belarus. (chaikov@dragon.bas-net.by)
- A. Comerón and M. Á. López Márquez, Universitat Politècnica de Catalunya, Departament TSC, Jordi Girona 1 y 3. Edificio D3-202, 08034 Barcelona, Spain. (comeron@tsc.upc.es; malopez@tsc.upc.es)
- S. Eckhardt and A. Stohl, Technische Universität München, Am Hochanger 13, 85354 Freising-Weihenstephan, Germany. (sabine@forst.tu-muenchen.de; as@forst.tu-muenchen.de)
- R. Eixmann, Leibniz-Institut für Atmosphärenphysik, Schlossstraße 6, 18225 Kühlungsborn, Germany. (eixmann@iap-kborn.de)
- V. Freudenthaler and M. Wiegner, Meteorologisches Institut der Ludwig Maximilians-Universität, Theresienstraße 37, 80333 München, Germany. (volker.freudenthaler@meteo.physik.uni-muenchen.de; m.wiegner@meteo.physik.uni-muenchen.de)
- P. Ginoux, NOAA Geophysical Fluid Dynamics Laboratory, Princeton, NJ 08542, USA. (paul.ginoux@noaa.gov)
- L. Komguem and G. Vaughan, Physics Department, University of Wales, Aberystwyth, Ceredigion SY23 3BZ, UK. (llk@aber.ac.uk; gxv@aber.ac.uk)
- V. Mitev and M. K. Srivastava, Observatoire de Neuchâtel, Rue de l'Observatoire 58, 2000 Neuchâtel, Switzerland. (valentin.mitev@ne.ch; manoj.srivastava@ne.ch)
- S. Music and S. Nickovic, Euro-Mediterranean Center on Insular Coastal Dynamics, University of Malta, St. Paul Street, Valletta, Malta. (s.music@icod.org.mt; nicko@icod.org.mt)
- J. Pelon, Service d'Aéronomie, Centre National de la Recherche Scientifique, Université Pierre et Marie Curie, Boîte 102, 4 place Jussieu, 75252 Paris Cedex, France. (jacques.pelon@aero.jussieu.fr)
- L. Sauvage, Institut Pierre Simon Laplace, Laboratoire de la Météorologie Dynamique, 91128 Palaiseau, France. (laurent.sauvage@lmd.polytechnique.fr)
- P. Sobolewsky, Institute of Geophysics, Polish Academy of Sciences, Ks. Janusza 64, Warsaw, 01-452 Poland. (pss@ra.onet.pl)
- O. Torres, NASA Goddard Space Flight Center and University of Maryland Code 916, Greenbelt, MD 20771, USA. (torres@tparty.gsfc.nasa.gov)

A. Ansmann, I. Mattis, D. Müller, and U. Wandinger, Leibniz Institute for Tropospheric Research, Permoserstraße 15, 04318 Leipzig, Germany. (albert@tropos.de; ina@tropos.de; detlef@tropos.de; ulla@tropos.de)